Chapter 12

Testing Effects of a Massive Graviton

The General Theory of Relativity has proven to be very predictive over the past century. As esoteric as it may seem, its effects can impact our every day lives, such as the General Relativistic corrections needed for GPS navigation to work. However, we know the predictions of General Relativity must break down at some small length scale since quantum effects will become important at the Planck scale.

General Relativity could also have flaws at large scales. It has also been observed that stars within galaxies and galaxies within galactic clusters orbit around the center of mass faster than they should based on the amount of visible matter [147, 148]. There are one of two conclusions that can be drawn from this, either there is more matter there than we can see, or General Relativity does not describe gravity at large distances.

Many people currently believe the former of these two options, positing the existence of dark matter to explain the missing mass. The latter option requires a modification to General Relativity at large distances, which could be accounted for in the form of a massive graviton.

In this chapter we will compare the analysis of Will [149] using 1.5PN waveforms to a new analysis using complete inspiral-merger-ringdown (IMR) waveforms. The rest of this chapter is as follows: we briefly summarize the effects of a massive graviton (section 12.1), give a dispersion relation for GWs in general (section 12.2) and specific to the analysis of GWs from CBC signals (section 12.3 and 12.4), use this dispersion relation to predict theoretical bounds for the mass of

the graviton from future CBC GW observations (section 12.5), and then compare these bounds to current observational bounds and theoretical bounds from other techniques (section 12.7).

12.1 Effects of Massive Gravitons

Endowing the graviton with mass would have many affects on different physical processes. These include changing the dispersion relation for gravitational waves such that they no longer travel at the speed of light [149], increasing the energy loss due to gravitational waves of a given frequency [150], and causing the Newtonian gravitational potential to have a Yukawa form instead of being $1/r$ which can affect the orbits of planets [149] and gravitational lensing observations [151]. The rest of this chapter will focus on the first of these effects expect the final section (section 12.7) where we compare these bounds to the bounds from other methods.

12.2 Dispersion of Gravitational Waves

In reference [149], Will derived the propagation effects for two GWs traveling over cosmological distances, which we repeat below. Let us distinguish these GWs using the presence or absence of a "$\prime$" on the properties of the two waves. Let us also denote properties of either wave at the time of emission with an e subscript and at the time of arrival or measurement with an a subscript. The emitted energies of these GWs is then given as E_e and E'_e and the emission time difference as $\Delta t_e \equiv t'_e - t_e$. For clarity, we also recover the G and c terms for formulae in this chapter.

Let us assume the GWs propagate in a flat Friedman-Robertson-Walker homogeneous and isotropic spacetime, with background metric given as

$$ds^2 = -c^2 dt^2 + a^2(t)\left[dr^2 + r^2\left(d\theta^a + \sin^2\theta d\phi^2\right)\right] , \tag{12.1}$$

where $a(t)$ is the expansion factor of the universe.

Consider a graviton moving radially with mass m, 4-velocity $u^\alpha = dx^\alpha/d\tau$, and 4-momentum

$p^\alpha = mu^\alpha$. Let it be emitted at a distance $r = r_e$ and detected at $r = 0$. The energy-momentum relation is given as

$$m^2c^4 = -p^\alpha p^\beta g_{\alpha\beta} = E^2 - a^{-2}p_r^2c^2 \ , \tag{12.2}$$

where $E = p^0c$ is the energy of the particle, m is the mass of the particle, and p_r is the particles radial momentum. Combining this with the ratio $p^rc/E = p^r/p^0 = dr/dt$, after eliminating E we find

$$\frac{dr}{dt} = -\frac{c}{a}\left(1 + \frac{a^2m_g^2c^2}{p_r^2}\right)^{-1/2} \ . \tag{12.3}$$

Since the graviton will be following a geodesic, its 4-velocity will satisfy the geodesic equation $u^\alpha{}_{;\mu}u^\mu = 0$. Using the property of the metric that $g^{\mu\nu}{}_{;\alpha} = 0$, we also know that $u_{\alpha;\mu}u^\mu = 0$. Expanding the covariant derivative using a Christoffel symbol, this is then given by $u_{\alpha,\mu}u^\mu - u_\nu u^\mu \Gamma^\nu{}_{\alpha\mu} = 0$. Expanding the Christoffel symbol and using its symmetries, we can write this as $u_{\alpha,\mu}u^\mu - u^\mu u^\nu g_{\mu\nu,\alpha} = 0$. Specializing this to u_r and using the fact that only the time and radial components of the 4-velocity u^α are nonzero, and both $g_{0\mu}$ and $g_{r\mu}$ are independent of r, we then find $u_{\alpha,\mu}u^\mu = 0$, which shows u^r to be conserved. This then implies that p_r is a conserved component of the 4-momentum. We choose to evaluate it at the moment of emission of the GW, $p_r^2c^2 = a^2(t_e)\left(E_e^2 - m_g^2c^4\right)$.

Using the relation from quantum mechanics between a wave's frequency f and its energy $E = hf$, where h is Planck's constant, and the definition of the Compton wavelength of a particle $\lambda \equiv h/m$, we find that $m_gc^2/E_e = c/(\lambda_g f_e)$. Let us assume that the lowest frequency we are interested in is such that $E_e \gg m_gc^2$. Then the dispersion relation above can be expanded to second order in $c/(\lambda_g f_e)$ as

$$\frac{dr}{dt} = -\frac{c}{a}\left(1 - \frac{c^2a^2}{2a^2(t_e)\lambda_g^2 f_e^2}\right) \ , \tag{12.4a}$$

which after integration gives

$$r_e = \int_{t_e}^{t_a} \frac{c}{a(t)}dt - \frac{c^3}{2a^2(t_e)\lambda_g^2 f_e^2}\int_{t_e}^{t_a} a(t)dt \ . \tag{12.4b}$$

Let us apply this to the two GW emitted with energies E_e and E_e' with a time difference of

$\Delta t_e \equiv t'_e - t_e$. Application to the first wave yields

$$r_e = \int_{t_e}^{t_a} \frac{c}{a(t)} dt - \frac{c^3}{2a^2(t_e)\lambda_g^2 f_e^2} \int_{t_e}^{t_a} a(t) dt \ , \tag{12.5a}$$

while application to the second yields

$$r_e = \int_{t_e+\Delta t_e}^{t_a+\Delta t_a} \frac{c}{a(t)} dt - \frac{c^3}{2a^2(t_e)\lambda_g^2 f_e'^2} \int_{t_e+\Delta t_e}^{t_a+\Delta t_a} a(t) dt \ . \tag{12.5b}$$

Combining these two results gives us

$$\begin{aligned} \int_{t_a}^{t_a+\Delta t_a} \frac{c}{a(t)} dt - \int_{t_e}^{t_e+\Delta t_e} \frac{c}{a(t)} dt &= \frac{c^3}{2\lambda_g^2} \left(\frac{1}{a^2(t_e+\Delta t_e) f_e'^2} \int_{t_e+\Delta t_e}^{t_a+\Delta t_a} a(t) dt \right. \\ &\left. - \frac{1}{a^2(t_e) f_e^2} \int_{t_e}^{t_a} a(t) dt \right) \ . \end{aligned} \tag{12.6}$$

This can be simplified even further in the case where the characteristic time it takes a to change is large compared to the emission time difference, characterized by $\Delta t_e \ll a/\dot{a}$, and where the time difference between t_e and t_a is large to the form

$$\Delta t_a = (1+Z) \left[\Delta t_e + \frac{Dc}{2\lambda_g^2} \left(\frac{1}{f_e'^2} - \frac{1}{f_e^2} \right) \right] \ , \tag{12.7}$$

where $Z \equiv a_0/a(t_e) - 1$ is the cosmological redshift, and D is a distance given by

$$D \equiv \frac{(1+Z)c}{a_0} \int_{t_e}^{t_a} a(t) dt \ , \tag{12.8}$$

where $a_0 \equiv a(t_a)$ is the present value of the expansion factor. D is different from standard cosmological distances, such as the luminosity distance $D_L \equiv a_0(1+Z)\chi_e$. For a matter-dominated spatially-flat universe, D and D_L are given by

$$D = \frac{2c}{5H_0}(1+Z) \left[1 - (1+Z)^{-5/2} \right] \ , \tag{12.9a}$$

$$D_L = \frac{2c}{H_0}(1+Z)\left[1-(1+Z)^{-1/2}\right] \ , \tag{12.9b}$$

where H_0 is the Hubble constant given by $c/H_0 \simeq 42$Gpc. Both cases reduce to the familiar Hubble law cZ/H_0 in the limit $Z \ll 1$. It should also be noted that the frequency upon arrival to the detector will have undergone a redshift such that $f_a = f_e/(1+Z)$.

12.3 Dispersion of Compact Binary Coalescence Gravitational Waveforms

This dispersion relation above, equation (12.4), tells us that GW of different frequencies will travel at different speeds. This can change the morphology of GW signals emitted from a single source that originally were emitted with a well-defined frequency evolution.

With this in mind, let us analyze what happens to the inspiral waveform we calculated in chapter 2, where the orbital phase evolution $\Phi(t)$ is given in equation (2.36b). Taking the time derivative of the phase evolution $2\Phi(t)$, we find the frequency evolution $\pi f(t) = d\Phi/dt$ to be

$$f(t) = \left(\frac{GM}{c^3\pi^2}\right)^{1/2}\left[\frac{5c^9}{256G^3M^3\eta\left(\frac{405GM}{16c^3\eta}+t_{\rm ISCO}-t\right)}\right]^{3/8} \ , \tag{12.10}$$

where $M = m_1 + m_2$ is the total mass of the system, $\eta = m_1m_2/M^2$ is the symmetric mass ratio, and we have defined $t_{\rm ISCO}$ to be the time when the frequency is that corresponding to the ISCO $f_{\rm ISCO} = c^3/(G6^{3/2}\pi M)$.

Let us consider equation (12.7) for two waves emitted at $t = t_{\rm ISCO} - \Delta t$ and $t' = t_{\rm ISCO}$ and find the distance D at which they will arrive at the same time (i.e., $\Delta t_a = 0$). Plugging these two times into equation (12.10), using the frequencies in equation (12.7), and solving for D where $\Delta t_a = 0$, we find

$$D = \frac{2\lambda_g^2\Delta t}{\frac{\pi^2}{5^{3/4}M}\left[256\eta M^3\left(\frac{405M}{16\eta}+\Delta t\right)\right]^{3/4} - 216\pi^2M^2} \ . \tag{12.11}$$

Taking the limit of this as $\Delta t \to 0$, we find the distance at which the end of the waveform starts to

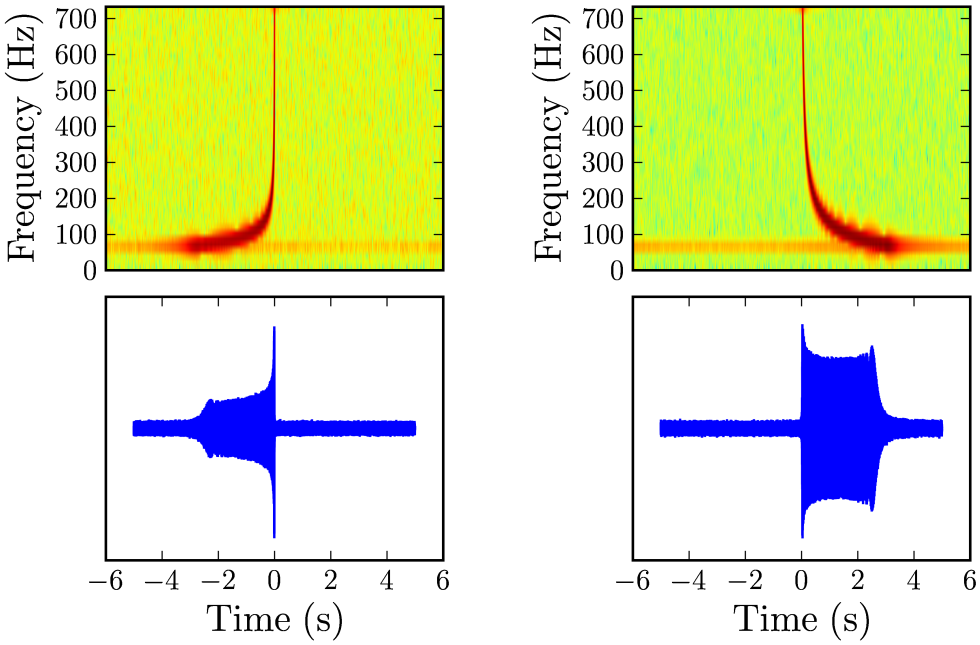

Figure 12.1: Waveform Inversion
Plots of inspiral waveforms at $D \ll D_{\rm inv}$ (left) and $D \gg D_{\rm inv}$ (right). The upper plots show spectrograms of the waveforms below. This makes it easier to see what frequency information arrives at what time.

become inverted ($D_{\rm inv}$) to be

$$D_{\rm inv} = \frac{5\lambda_g^2}{16\pi^2\eta M} \,. \tag{12.12}$$

Different waveforms are plotted in figure 12.1 showing how the morphology of the GW wave changes as it propagates due to dispersion effects of a massive graviton. The end of the waveform starts becoming inverted at $D \sim D_{\rm inv}$. At $D \gg D_{\rm inv}$, the information at the end of the waveform (i.e., the higher frequency portion of the waveform) can be seen to arrive before information that was emitted earlier (i.e., the lower frequency portion of the waveform).

12.4 Recovery of Dispersed Compact Binary Coalescence Gravitational Waveforms

In chapter 2 we found the inspiral portion of CBC waveforms as a function of time. Converted to the form found in [149], these are given as

$$h(t) = A(t)e^{-i\Phi(t)} \,, \tag{12.13a}$$

$$\Phi(t) = \Phi_0 + 2\pi \int_{t_c}^{t} f(t)dt \,, \tag{12.13b}$$

$$A(t) = \frac{\mathcal{M}}{D_L}\left(\frac{5\mathcal{M}}{t_c - t}\right)^{1/4} \,. \tag{12.13c}$$

When searching for these signals in GW detector data, as discussed in chapter 2, it is convenient to convert these waveforms to the frequency domain using the SPA (equation (2.41)). Converting the SPA phase (equation (2.45)) to the form found in [149], $\Psi(f)$ is given as

$$\Psi(f) = 2\pi \int_{f}^{f_c} (t_c - t)df' + 2\pi f t_c + \phi_0 \,, \tag{12.14}$$

where the subscript c denotes a value at the time of coalescence. These waveforms are used to search for signals in the GW detector data with the technique known as matched filtering (discussed in chapter 5) where an inner product is defined as

$$(h_1|h_2) = 4\Re\left[\int_0^\infty \frac{\tilde{h}_1^* \tilde{h}_2}{S_n(f)} df\right] \,, \tag{12.15}$$

where $\Re[\cdots]$ denotes the real part of $[\cdots]$, $\tilde{h}^*$ denotes the complex conjugate of $\tilde{h}$, and $S_n(f)$ is the power spectral density of the particular detector.

Since these are the waveforms that are used for the detection of signals, all of the f's above are measured frequencies, which as we have stated above, are related to the emitted frequencies by $f = f_e/(1+Z)$. We are now in a position to see how the massive graviton propagation effects change a signal of the form given in equation (2.41). The term which is modified by these effects is the

integral term in the phase $\Psi(f)$ (equation (12.14)). Applying equation (12.7) to this term we find it changes to be

$$\begin{aligned}\int_f^{f_c}(t_c-t)df' &= \int_{f_e}^{f_{ec}}(t_{ec}-t_e)df'_e+\int_{f_e}^{f_{ec}}\frac{D}{2\lambda_g^2 f_e'^2}df'_e-\int_{f_e}^{f_{ec}}\frac{D}{2\lambda_g^2 f_{ec}^2}df'_e \\ &= \int_{f_e}^{f_{ec}}(t_{ec}-t_e)df'_e-\frac{D}{2\lambda_g^2 f_e}+\frac{D}{\lambda_g^2 f_{ec}}-\frac{D}{2\lambda_g^2 f_{ec}^2}f_e\,. \end{aligned} \tag{12.16}$$

These additional terms can be seen to have different effects on the waveform. The last term has an f_e^1 dependence, which is the same dependence as the time offset term in equation (12.14) and can be interpreted as a change in the arrival time. The second-to-last term has an f_e^0 dependence, which is the same dependence as the phase offset term in equation (12.14) and can be interpreted as a change in the phase at coalescence. The other additional term (the second term) has an f_e^{-1} dependence, which is the same as the 1.0PN phase term. This is the term that will change the morphology of the waveform. Its effect on equation (2.45) is to add an additional $-\beta f^{-1}$ term, where $\beta \equiv \frac{\pi D}{\lambda_g^2(1+Z)}$. To 1.5PN order, $\Psi(f)$ is then given as

$$\begin{aligned}\Psi(f) &= 2\pi f t_c+\phi_0-\frac{3}{128\eta}\left[(\pi Mf)^{-5/3}+\left(\frac{3715}{756}+\frac{55}{9}\eta\right)(\pi Mf)^{-1}\right. \\ &\quad \left.-16\pi\,(\pi Mf)^{-2/3}\right]-\beta f^{-1}\end{aligned} \tag{12.17}$$

12.5 Using the Dispersion of Gravitational Waves to Bound the Mass of the Graviton

In reference [149], Will used the above formalism with restricted inspiral waveforms to 1.5PN order in the phase to predict bounds on the mass of the graviton from the detection of signals from Adv. LIGO and LISA. Will's analysis used the rms error of associated massive graviton phase term from parameter estimation techniques. Specifically, the rms error of a parameter θ^α is given by

$$\Delta\theta^\alpha \equiv \sqrt{\left\langle\left(\theta^\alpha-\langle\theta^\alpha\rangle\right)^2\right\rangle}=\sqrt{\Sigma^{\alpha\alpha}}\,, \tag{12.18}$$

where Σ is the inverse of the Fischer Information matrix Λ given by

$$\Lambda_{\alpha\beta} \equiv \left(\frac{\partial h}{\partial \theta^\alpha} | \frac{\partial h}{\partial \theta^\beta} \right) . \tag{12.19}$$

For this analysis, we will compare the results of Will's analysis [149] using 1.5PN waveforms to a similar analysis using new IMR waveforms. The IMR waveforms we use are frequency domain phenomenological waveforms whose phenomenological parameters have been tuned using Numerical Relativity waveforms with symmetric mass ratios $0.25 \geq \eta \geq 0.16$ [152, 153]. These waveforms are given by

$$\tilde{h}(f) \equiv A_{\rm eff}(f) e^{i\Psi_{\rm eff}(f)} , \tag{12.20}$$

where the effective amplitude $A_{\rm eff}(f)$ and phase $\Psi_{\rm eff}$ are given by

$$A_{\rm eff}(f) \equiv C \begin{cases} (f/f_1)^{-7/6} & \text{if } f < f_1 \\ (f/f_1)^{-2/3} & \text{if } f_1 \leq f < f_2 \\ w\mathcal{L}(f, f_2, \sigma) & \text{if } f_2 \leq f < f_3 \\ 0 & \text{if } f \geq f_3 , \end{cases} \tag{12.21a}$$

$$\Psi_{\rm eff}(f) \equiv 2\pi f t_0 + \phi_0 + \sum_{k=0}^{6} \psi_k f^{(k-5)/3} , \tag{12.21b}$$

where $C = \frac{M^{5/6} f_1^{-7/6}}{D_L \pi^{2/3}} \sqrt{\frac{5\eta}{24}}$ is the amplitude parameter for optimally oriented and located sources, $w = \frac{\pi\sigma}{2} \left(\frac{f_2}{f_1} \right)^{-2/3}$ is a normalization such that $A_{\rm eff}$ is continuous through f_2, $\mathcal{L}(f, f_2, \sigma) = \frac{1}{2\pi} \frac{\sigma}{(f-f_2)^2 + \sigma^2/4}$ is a Lorentzian function centered on f_2 with width σ, t_0 is the arrival time, and ϕ_0 is the phase offset. For these waveforms, f_1 corresponds to the where the PN amplitude evolution ends (i.e., where the inspiral ends and the merger begins), f_2 corresponds to where the merger ends and the ringdown begins, and f_3 is the frequency at which we cut off the waveform. The ringdown portion of the waveform is modelled as a Lorentzian which agrees with the quasi-normal mode ringing of a perturbed black hole from black hole perturbation theory.

The phenomenological amplitude parameters $\alpha_k = \{f_1, f_2, f_3, \sigma\}$ are given by

$$\alpha_k = \frac{a_k\eta^2 + b_k\eta + c_k}{\pi\mathcal{M}}\eta^{3/5} , \tag{12.22a}$$

where a_k, b_k, and c_k are given in Table 12.1. The phenomenological phase parameters ψ_k are given by

$$\psi_k = \frac{x_k\eta^2 + y_k\eta + z_k}{(\pi\mathcal{M})^{(5-k)/3}}\eta^{-k/5} , \tag{12.22b}$$

where x_k, y_k, and z_k are given in Table 12.1. The phenomenological phase parameters do not match the PN terms because of the choice of the authors in references [152, 153]. They allowed these terms to vary while trying to maximize the "faithfulness" and "effectualness" of the phenomenological waveforms to recovering hybrid PN-Numerical Relativity waveforms.

Table 12.1: Phenomenological Coefficients

Parameter	a_k	b_k	c_k
f_1	6.6389 $\times10^{-1}$	-1.0321 $\times10^{-1}$	1.0979 $\times10^{-1}$
f_2	1.3278	-2.0642 $\times10^{-1}$	2.1957 $\times10^{-1}$
σ	1.1383	-1.7700 $\times10^{-1}$	4.6834 $\times10^{-2}$
f_3	1.7086	-2.6592 $\times10^{-1}$	2.8236 $\times10^{-1}$
Parameter	x_k	y_k	z_k
ψ_0	-1.5829 $\times10^{-1}$	8.7016 $\times10^{-2}$	-3.3382 $\times10^{-2}$
ψ_2	3.2967 $\times10^{1}$	-1.9000 $\times10^{1}$	2.1345
ψ_3	-3.0849 $\times10^{2}$	1.8211 $\times10^{2}$	-2.1727 $\times10^{1}$
ψ_4	1.1525 $\times10^{3}$	-7.1477 $\times10^{2}$	9.9692 $\times10^{1}$
ψ_6	1.2057 $\times10^{3}$	-8.4233 $\times10^{2}$	1.8046 $\times10^{2}$

Unitless coefficients describing the amplitude and phase of the phenomenological waveforms from reference [152] to be used in equations (12.22). There is no ψ_1 term as the 0.5PN phasing term is 0.

The amplitude C given above is the amplitude one would find for an optimally oriented and optimally located source. Averaging over random angles for the two sky location angles, the polarization angle, and the inclination angle, there is an overall factor of $2/5$ we should apply to this. For this reason we redefine $C = \frac{2M^{5/6}f_1^{-7/6}}{5D_L\pi^{2/3}}$ from here on.

Applying equation (12.16) to this waveform results in a measured phase evolution of

$$\Psi_{\rm eff}(f) \equiv 2\pi f t_0 + \phi_0 + \sum_{k=0}^{6}\psi_k f^{(k-5)/3} - \beta f^{-1} , \tag{12.23}$$

where t_0 is the measured arrival time which has absorbed the massive graviton term with the f^1 dependence and ϕ_0 is the measured phase offset which has absorbed the massive graviton term with the f^0 dependence.

In producing this result, we have made an assumption which we must check. This is that, at the order to which we the phase evolution of the binary, energy loss due to massive graviton effects are negligible. Since we use phenomenological terms up to the equivalent 3.0PN order and ignore massive graviton effects of order $(r/\lambda_g)^2$ when computing the energy loss at the source, this implies we require $r^2\lambda_g^{-2}v^{-6} \ll 1$. Combining this with $v^2 \sim M/r$ and $v = 2\pi r f$, we find the frequencies this holds for are $f > \lambda_g^{-3/5}M^{-2/5}/(2\pi)$, which is $f > 2.6 \times 10^{-3}(M/M_\odot)^{-2/5}$Hz assuming the current bound on $\lambda_g > 10^{12}$ km. For the systems we consider, this is always satisfied.

The parameters we use in the Fischer Matrix calculation are $\ln C$, ϕ_0, t_0, $\ln \mathcal{M}$, $\ln \eta$, and β. The partial derivatives of $\tilde{h}$ with respect to these are given by

$$\frac{\partial \tilde{h}(f)}{\partial \ln C} = \tilde{h}(f) \,, \tag{12.24a}$$

$$\frac{\partial \tilde{h}(f)}{\partial \phi_0} = -i\tilde{h}(f) \,, \tag{12.24b}$$

$$\frac{\partial \tilde{h}(f)}{\partial t_0} = 2\pi i\tilde{h}(f) \,, \tag{12.24c}$$

$$\frac{\partial\tilde{h}(f)}{\partial\ln\mathcal{M}} = Ce^{i\Psi_{\rm eff}}\begin{cases}\frac{7}{6}\frac{\partial\ln f_1}{\partial\ln\mathcal{M}}\left(\frac{f}{f_1}\right)^{-7/6} & \text{if } f<f_1\\ \frac{2}{3}\frac{\partial\ln f_1}{\partial\ln\mathcal{M}}\left(\frac{f}{f_1}\right)^{-2/3} & \text{if } f<f_1\\ w\mathcal{L}(f,f_2,\sigma)\left(\frac{\partial\ln w}{\partial\ln\mathcal{M}}+\frac{\partial\ln\mathcal{L}(f,f_2,\sigma)}{\partial\ln\mathcal{M}}\right) & \text{if } f_2\le f<f_3\\ 0 & \text{if } f\ge f_3\end{cases}$$
$$+ iCe^{i\Psi_{\rm eff}}\sum_{k=0}^{6}\left[\psi_k\frac{\partial\ln\psi_k}{\partial\ln\mathcal{M}}f^{(k-5)/3}\right]\begin{cases}(f/f_1)^{-7/6} & \text{if } f<f_1\\ (f/f_1)^{-2/3} & \text{if } f_1\le f<f_2\\ w\mathcal{L}(f,f_2,\sigma) & \text{if } f_2\le f<f_3\\ 0 & \text{if } f\ge f_3\,,\end{cases} \tag{12.24d}$$

$$\frac{\partial\tilde{h}(f)}{\partial\ln\eta} = Ce^{i\Psi_{\rm eff}}\begin{cases}\frac{7}{6}\frac{\partial\ln f_1}{\partial\ln\eta}\left(\frac{f}{f_1}\right)^{-7/6} & \text{if } f<f_1\\ \frac{2}{3}\frac{\partial\ln f_1}{\partial\ln\eta}\left(\frac{f}{f_1}\right)^{-2/3} & \text{if } f<f_1\\ w\mathcal{L}(f,f_2,\sigma)\left(\frac{\partial\ln w}{\partial\ln\eta}+\frac{\partial\ln\mathcal{L}(f,f_2,\sigma)}{\partial\ln\eta}\right) & \text{if } f_2\le f<f_3\\ 0 & \text{if } f\ge f_3\end{cases}$$
$$+ iCe^{i\Psi_{\rm eff}}\sum_{k=0}^{6}\left[\psi_k\frac{\partial\ln\psi_k}{\partial\ln\eta}f^{(k-5)/3}\right]\begin{cases}(f/f_1)^{-7/6} & \text{if } f<f_1\\ (f/f_1)^{-2/3} & \text{if } f_1\le f<f_2\\ w\mathcal{L}(f,f_2,\sigma) & \text{if } f_2\le f<f_3\\ 0 & \text{if } f\ge f_3\,,\end{cases} \tag{12.24e}$$

$$\frac{\partial\tilde{h}(f)}{\partial\beta} = -if^{-1}\tilde{h}(f)\,. \tag{12.24f}$$

When taking the inner products in calculating Λ, we find it is helpful to introduce the definition

ofof an integral $I_a^b(p,q)$ given by

$$I_a^b(p,q) \equiv 4\int_a^b \frac{f^{-p/3}}{((f-f_2)^2+\sigma^2/4)^q\, g_\alpha(f)} df \ , \tag{12.25}$$

where $g_\alpha(f)$ is the frequency dependence of the detectors PSD. The PSD can then be written as $S_n(f) = S_0 g_\alpha(f)$. In this notation, the SNR can be written as

$$\begin{aligned} \rho &\equiv (h|h)^{1/2} \\ &= \frac{C}{\sqrt{S_0}}\left[f_1^{7/3} I_0^{f_1}(7,0) + f_1^{4/3} I_{f_1}^{f_2}(4,0) + \frac{w^2\sigma^2}{4\pi^2} I_{f_2}^{f_3}(0,2)\right]^{1/2} . \end{aligned} \tag{12.26}$$

In the calculation of the inverse of the Fischer Matrix, we find all of the terms to be proportional to $\sqrt{S_0}/C$. Let us then define Δ as $\Delta\beta \equiv \Delta^{1/2}\sqrt{S_0}/C$. In setting an upper limit on the mass of the graviton, we view $\Delta\beta$ as the upper bound on β which results in a lower bound on λ_g given by

$$\lambda_g > \left(\frac{D}{(1+Z)D_L}\right)^{1/2}\left(\frac{\pi^2 C\mathcal{M}}{S_0^{1/2}\Delta^{1/2}}\right)^{1/2} . \tag{12.27}$$

In Table 12.2 we summarize the bounds on λ_g we obtain from the complete IMR waveforms and compare them to the results from Will [149]. This table uses two different noise models, one for signals which Adv. LIGO will be sensitive to, and one for signals LISA will be sensitive to. The noise model for Adv. LIGO is given by $S_0 = 3\times10^{-48}$ and $g_\alpha(f) = ((f/f_n)^{-4} + 2 + 2(f/f_n)^2)/5$ where $f_n = 70$Hz. Since Adv. LIGO is sensitive down to $f_0 = 40$Hz, this is where we start the integration instead of at 0Hz. The noise model for LISA is given by $S_0 = 4.2\times10^{-41}$ and $g_\alpha(f) = (10^{1/2}(f/f_n)^{-14/3} + 1 + (f/f_n)^2/1000 + 313.5(f/f_n)^{-(6.398+3.518\log_{10}x)})$ where $f_n = 10^{-3}$Hz. For LISA, we start the integration at the lower frequency corresponding to a $T = 1$yr integration time, such that $f_0 = (5\mathcal{M}T^{-1}/256)^{3/8}/(\pi\mathcal{M})$.

We see from table 12.2 and figure 12.2 that for some signals, we can obtain better bounds from the PN inspiral-only waveform than from the complete IMR waveform. If we repeat the above analysis for the phenomenological waveform keeping only the inspiral portion with the $f^{-7/6}$

Table 12.2: Massive Graviton Bounds

m_1 ($M_\odot$)	m_2 ($M_\odot$)	Detector	Distance (Mpc)	Inspiral Bound (km)	Complete Waveform Bound (km)
10	10	Adv. LIGO	1500	6.0×10^{12}	4.8×10^{12}
50	50	Adv. LIGO	3000	2.8×10^{12}	4.8×10^{13}
10^4	10^4	LISA	3000	7.4×10^{15}	4.3×10^{15}
10^5	10^5	LISA	3000	2.3×10^{16}	1.1×10^{16}
10^6	10^6	LISA	3000	5.4×10^{16}	2.1×10^{17}
10^7	10^7	LISA	3000	6.9×10^{16}	5.1×10^{17}
10^8	10^8	LISA	3000	5.8×10^{16}	9.7×10^{17}
10^9	10^9	LISA	3000	2.6×10^{16}	1.1×10^{18}

The theoretical bounds on λ_g that could be placed based on a GW detection from different mass CBC signals. The column "Inspiral Waveform" refers to the bounds one could get from just looking at the inspiral portion of the waveform up to the ISCO frequency. Where available, these agree quantitatively with Will [149]. The column "Full Waveform" refers to the bounds one could get from looking at the complete IMR waveform which has been characterized by Ajith [152] and Ajith et al. [153].

amplitude frequency dependence and setting the cutoff frequency to be $f_{\rm ISCO}$, we find that the PN waveform always beats the phenomenological waveform. This is due to the differences between the phenomenological phasing parameters and the PN phasing parameters Ajith et al. noted in [153]. The above observation implies the parameters of the PN waveform are less degenerate than the parameters of the phenomenological waveform.

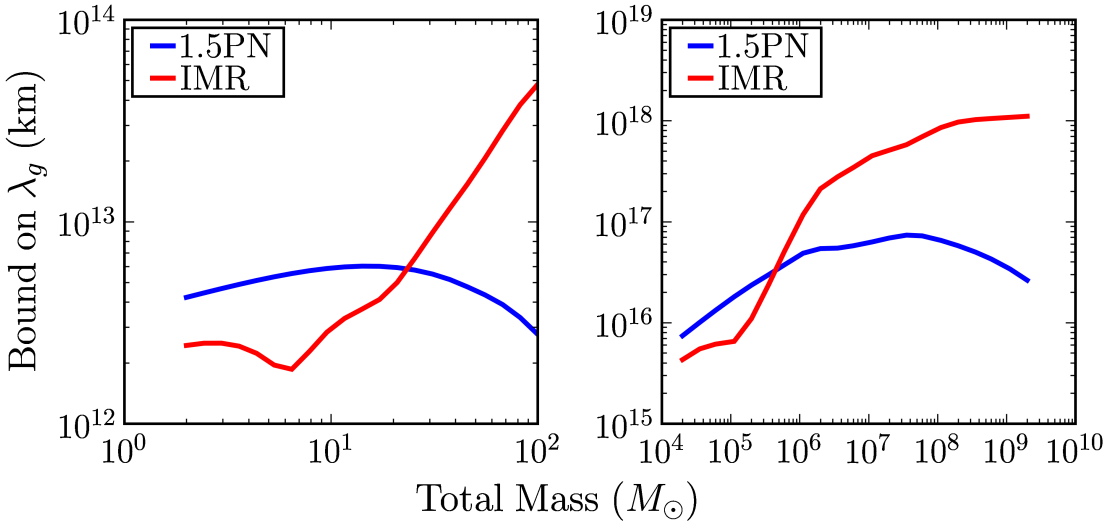

Figure 12.2: Massive Graviton Bounds
Plots of theoretical bounds on λ_g that could be placed based on a GW detection from Adv. LIGO mass systems (left) and LISA mass systems (right). For each mass of the Adv. LIGO systems, the bound was calculated using lesser of the distance corresponding to an SNR of 10 for the 1.5PN waveform and a distance of 3 Gpc and a minimum frequency of 10 Hz. For each mass of the LISA systems, the bound was calculated using a distance of 3 Gpc and a bandwidth corresponding to 1 year of integration time. The 1.5PN curves correspond to the bounds one could get from just looking at the 1.5PN waveform up to the ISCO frequency, as was done in Will [149]. The IMR curves correspond to the bounds one could get from looking at the complete IMR waveform which has been characterized by Ajith [152] and Ajith et al. [153].

12.6 Beyond the Fischer Matrix Approach

The approach that has been taken by Will [149] and here to constrain the mass of the graviton is the Fischer information matrix approach. This approximation is only valid in the large SNR limit and does not include known issues involved in real data analysis pipelines, which search for inspiral signals, such as recovery of a signal with incorrect parameters and separating the amplitude correlations between distance, mass, and sky location. A full simulation is required to accurately determine the achievable bounds on the mass of the graviton with one, or even several, observed signals.

12.7 Other Bounds on the Graviton's Mass

Let us compare these results to the results available from other physical effects of a massive graviton. The first effect we shall look at is changes in planetary motion due to a Yukawa gravitational potential. If this were the case, Kepler's third law would be violated since the gravitational force would no longer follow an inverse-square law. This leads to a bound on the mass of the graviton in the form of $\lambda_g > (\frac{1-a_p^2}{6\eta_p})^{1/2}$ where a_p is the semimajor axis of planet p, η_p is planet p's bound on the η parameter given by Talmadge et al. [154]. Both λ_g and a_p are given in astronomical units. The most stringent bound of this form comes from the orbit of Mars which limits the mass of the graviton such that $\lambda_g > 2.8 \times 10^{12}$ km [149].

The next bound on the mass of the graviton is from binary pulsar observations. If the graviton had mass, the orbits of binary pulsars would decay at a slightly faster rate than predicted by General Relativity, due to additional energy loss from the leading order massive graviton terms in the power radiated. Combining the observations of PSR B1913+16 and PSR B1534+12, the 90% confidence bound on the mass of the graviton is $\lambda_g > 1.6 \times 10^{10}$ km [150].

The final bound on the mass of the graviton we shall look at can be obtained by studying gravitational lensing data. Assuming a specific distribution of dark matter, lensing data can be studied looking for an effect which would change the distribution of the variance of the power

spectrum $\gamma^2(\theta)$ smoothed over a filter of radius θ. When comparing the predictions of a $1/r$ potential versus the Yukawa potential, Choudury et al. [151] find the bound on the mass of the graviton to be $\lambda_g > 3 \times 10^{21}$ km [151]. However, this upper limit is less robust than the others above as one must assume a specific distribution of dark matter before calculating the bound.